Journal of the Ceramic Society of Japan 119 [4] 255-260 2011 Special Article
The 64th CerSJ Awards for Advancements in Ceramic Science and Technology: Review

Synthesis and characterization of Si-based materials: zeolites and SiAlONs

Toru WAKIHARA†

Department of Environmental and Information Sciences, Yokohama National University, 79–7 Tokiwadai, Hodogaya-ku, Yokohama 240–8501

Zeolites have been utilized widely in industry and in household products, for example, as adsorbents, ion-exchangers and catalysts, and have attracted considerable attention as host materials for various recent nanotechnology applications. The SiAlON ceramics, of which α-SiAlON and β-SiAlON are representative phases, are useful for engineering applications because of their excellent mechanical and chemical properties. This review introduces the author's contributions to the synthesis and characterization of these Si-based materials.

Key-words : Zeolite, Sialon, Si-based material, Nitridation, Diffraction

[Received November 1, 2010]

1. Introduction

Zeolites are hydrated, crystalline tectoaluminosilicates that are constructed from TO_4 tetrahedra (T = tetrahedral atom, e.g. Si and Al).[1)–4)] They contain well-ordered, nanometer-sized void spaces (ca. 3–15 Å) in their structures. **Figure 1** shows two typical zeolite structures, the LTA (zeolite A) and FAU (faujasite) type. Synthesis of artificial zeolites commenced in 1945, and to date, more than 190 framework structures have been recognized for zeolites and related materials including tectosilicates and tectoaluminophosphates.[5)] Most zeolites have been synthesized under hydrothermal conditions and the synthetic zeolites are produced as "metastable phases" in a thermodynamic sense. For example, in the Na_2O–Al_2O_3–SiO_2–H_2O system, albite, analcime, natrolite, nepheline, sodalite and montmorillonite, which are so-called "dense phases", are often formed at 300–700°C. At temperatures lower than 200°C, however, different zeolites (e.g. zeolite A and faujasite) are formed as metastable phases. Since there are many metastable phases under certain conditions, the products are sometimes obtained as a mixture. Therefore, from an industrial point of view, techniques for the synthesis of zeolite as a single phase are very important; for example, Kasahara et al.[6)] reported a process for the large-scale synthesis of pure faujasite. Zeolite molecular sieving capabilities have enabled their use as adsorbents, ion-exchangers and molecular-sieving membranes. Their acidic properties provide the basis for heterogeneous acid catalysis used in the petroleum and chemical industries.[7)] Furthermore, in recent years, research into novel applications of zeolites has been reported, such as in optical and magnetic applications,[8)–12)] based on their unique and regular structures as host frameworks for molecules, ions, and clusters.

The α- and β-SiAlONs are essentially solid solutions of α-Si_3N_4 and β-Si_3N_4 that have had some of their Si and N atoms replaced by Al and O, respectively. Certain metal cations, such as Li, Ca, Mg, Y and the rare-earth ions, are included in the large interstitial sites of α-SiAlON to maintain charge neutrality.[13)] These solid solutions have the formulae $M_xSi_{12-m-n}Al_{m+n}O_nN_{16-n}$ (α-SiAlON, $x = m/v$, v: cation charge) and $Si_{6-z}Al_zO_zN_{8-z}$ (β-SiAlON, $0 < z \leq 4.2$), respectively (see Fig. 1). SiAlON ceramics exhibit high strength and hardness, and are highly resistant to oxidation and corrosion, due to a wide variety of microstructures and properties, depending on the compositions and sintering parameters.[14),15)]

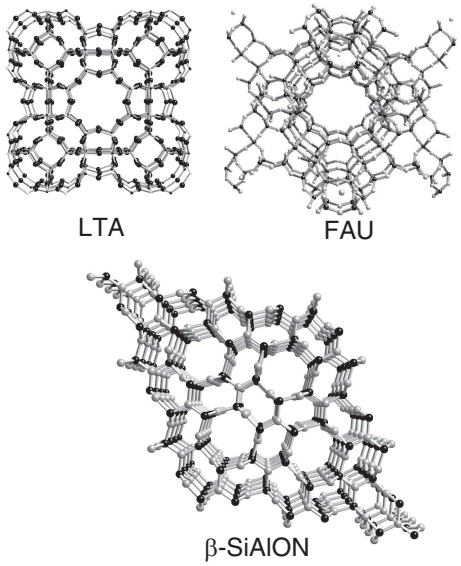

Fig. 1. Framework structure of LTA, FAU and β-SiAlON.

In general, the fabrication of both zeolites and SiAlONs are readily affected by various experimental factors [e.g. starting composition, synthesis (firing) temperature, mixing procedure and synthesis (firing) time]. Therefore, the formation mechanisms of zeolites and SiAlONs are not well understood, and their elucidation and control are still one of the major topics in materials science. This review summarizes the author's contributions to the synthesis and characterization of these Si-based materials.

† Corresponding author: T. Wakihara; E-mail: wakihara@ynu.ac.jp

2. Application of high-energy X-ray diffraction technique for the elucidation of zeolite crystallization[16)–20)]

Recent developments in analytical methods have enabled detailed studies of the crystallization mechanism of zeolites.[3)] Several attempts have been made over the years, using various techniques including NMR[21)–26)] (branched units of silicates, Si/Al ratio), conventional X-ray diffraction,[27)–29)] optical microscopy (morphology),[30)] dynamic light scattering (DLS; particle size distribution),[31),32)] small-angle X-ray/neutron scattering (particle size distribution),[33)–37)] transmission electron microscopy (TEM; inner and terminal structures),[38),39)] Raman spectroscopy (local structure)[40)–43)] and atomic force microscopy (AFM; surface structure).[44)–47)] Although these studies uncovered the crystallization of zeolites, they could not provide information regarding changes in the atomic arrangement from the amorphous to the crystalline phase. Diffraction methods (either X-ray or neutron) are commonly used to obtain the atomic arrangement[48)] of disordered materials. Although neutron diffraction is a valuable technique used for obtaining similar information, it is mainly sensitive to O–O correlations and in addition a small amount of hydrogen present in sample uncertainties in the data normalization.[49)] X-ray diffraction is well-suited for determining the atomic arrangement of disordered materials, in particular for extracting the T–T (T: Si, or Al) correlations, which are very important in determining the medium-range order of zeolite precursors. To analyze the structure of disordered materials using diffraction methods, it is necessary to obtain the structure factor, $S(Q)$, in a wide scattering vector Q ($Q = 4\pi \sin\theta/\lambda$, θ: scattering angle, λ: wavelength of photons or neutrons), since the resolution in the real space function depends on Q_{max} of the Fourier transformation of $S(Q)$. It is essential, therefore, to conduct measurements at high energies (very low wavelength of ca. 0.2 Å, which is now possible using third generation synchrotron radiation sources).

In this study, high-energy X-ray diffraction (HEXRD) experiments were carried out to elucidate the crystallization mechanisms of various zeolites on a horizontal two-axis diffractometer, optimized for structural measurements in glass and liquid, built at the BL04B2 high-energy monochromatic bending magnet beam line of SPring-8 (energy: 61.63 keV; wavelength: 0.2012 Å). The Q_{max} obtained in this study is 25 Å^{-1}. The data collected were subjected to well-established analysis procedures including absorption, background and Compton scattering corrections followed by normalization to the Faber–Ziman total structure factor, $S(Q)$. The total correlation function, $T(r)$, is derived from Eq. (1),

$$T(r) = 4\pi\rho r + \frac{2}{\pi}\int_{Q_{min}}^{Q_{max}} \{Q[S(Q) - 1]\sin(Qr)\}\mathrm{d}Q \quad (1)$$

where ρ is the total number density.

Figure 2 shows typical XRD spectra of the products formed in the synthesis of faujasite.[17)] No Bragg diffraction occurs in sample 1 (synthesis period: 1 h). An amorphous/crystalline mixture is obtained after 5 h of hydrothermal synthesis (sample 2), and the crystallization is complete after 24 h of hydrothermal synthesis (sample 3). **Figure 3** shows FE-SEM images of samples 1, 2 and 3. Only particles 100–300 nm in size (amorphous phase) are observed in sample 1, whereas faujasite crystals are observed among these amorphous particles in sample 2. A regular octahedron-shaped crystalline faujasite without amorphous phase is seen in sample 3, indicating that the

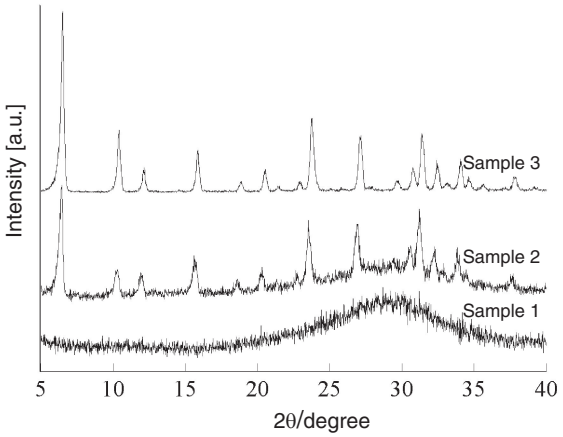

Fig. 2. XRD spectra of samples for the synthesis of faujasite; indicating that faujasite were formed from the amorphous phase. Note that all Bragg peaks are due to faujasite.

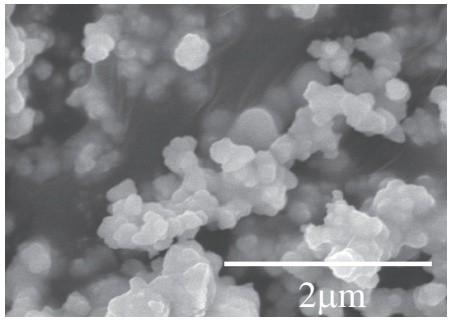

Sample 1

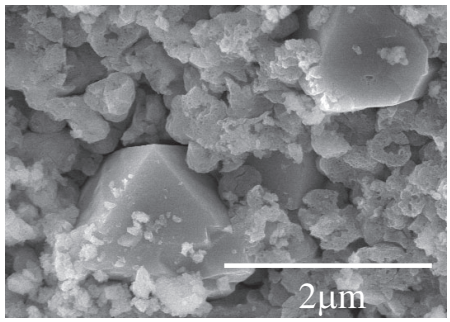

Sample 2

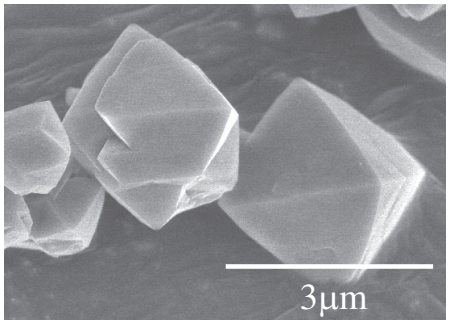

Sample 3

Fig. 3. FE-SEM image of samples 1, 2 and 3 for the synthesis of faujasite.

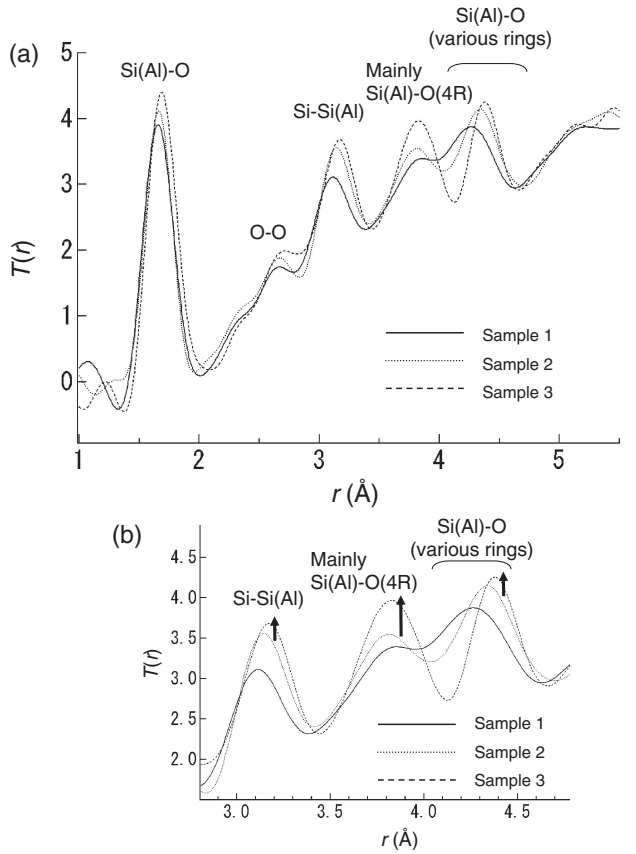

Fig. 4. (a) Total correlation functions, $T(r)$s, of samples 1, 2 and 3. (b) Magnified image of (a).

crystallization was completed at this stage. To extract quantitative information from the HEXRD data regarding the atomic arrangement in the amorphous and/or crystalline materials, the total correlation functions are calculated by the Fourier transformation of the total structure factor, $S(Q)$.

$T(r)$s of samples 1, 2 and 3 are shown in **Fig. 4**. From these functions, it is possible to identify the various distances, r(Å)s, associated with several features. The first peak in the $T(r)$ curves relates to Si–O and Al–O distances. The Q range obtained here is not sufficient to resolve the two distances of ca. 1.61 and 1.73 Å for tetrahedrally-coordinated Si and Al species, respectively. Distinct features are seen around 2.6 and 3.1 Å which are due to O–O and Si–Si(Al) correlations, respectively. As can be seen from Fig. 4, a peak is observed at 3.8 Å in the amorphous phase, which is mainly due to the second nearest neighbour to Si(Al)–O in 4R. The peak at 4.3 Å in the amorphous phase is mainly due to the second nearest neighbour to Si(Al)–O in various rings larger than 4R. Since the amorphous phase for the synthesis of faujasite contains a large fraction of 6R as reported in a previous study which used UV-Raman spectroscopy,[50] it appears that the peak at 4.3 Å is mainly due to 6R, and the peak shift in 4.3–4.4 Å during the crystallization is mainly due to the ordering of distorted 6R. The morphologies of amorphous aluminosilicates and crystalline zeolites are obviously different from one other as shown in Fig. 3. The crystallization of faujasite (at least the crystal growth), therefore, seems to proceed via the solution-mediated transport process under this condition. It should be noticed that the formation (ordering) of 4R occurs at a later stage than that of 6R, as shown in Fig. 4(b). If there are no changes in the structure of amorphous gel during the crystallization, and amorphous gel is simply a supplier of soluble species (if sample 2 is a mixture of sample 1 and sample 3), the difference in peak intensities should not occur [peak at 3.8 Å in sample 2 should be higher than that shown in Fig. 4(b)]. This result shows that the amorphous gel structure is changing towards that of the final crystalline phase during the crystallization.

As a result, a HEXRD technique for the elucidation of zeolite crystallization has been applied for the first time and clear changes are confirmed in the medium-range order, especially in the formation of aluminosilicate rings in the initial stages of zeolite crystallizations (zeolite A, zeolite X, mordenite and ZSM-5). Furthermore, HEXRD in combination with Reverse Monte Carlo modeling can provide information on more accurate atomic arrangements of the precursor particles.[16] This work is still in progress, and results are likely to elucidate the structural pathway for the formation of microporous materials.

3. Control of zeolite growth using dilute aluminosilicate solutions[51)–54)]

Recently, research on zeolites has been reported for the novel application of their unique structures as host frameworks for molecules, ions, and clusters. The author has focused on the preparation of oriented films of zeolites by heteroepitaxial growth for use in these potential applications. The ability to connect heterogeneous zeolite structures also enables the construction of multidimensional, nanospatial networks. Such nanospatial networks may serve as hosts to integrate molecular electronics and other molecular devices within their structures. Sodalite and cancrinite have structural similarities, since their aluminosilicate layers of six-membered rings are identical to one other. The differences in the structures originate from the stacking sequences of the six-membered rings. Sodalite along ⟨111⟩ is constructed by an "abc" stacking sequence, while cancrinite along [0001] is by an "ab" stacking sequence. In the same way, chabazite is also constructed from six-membered ring layers with a stacking sequence of "aabbcc" along [111]. First, the author showed the heteroepitaxial growth of hexagonal cancrinite on a millimeter-sized cubic sodalite single crystal [see **Fig. 5**(a)].[51),52)] A characteristic point of the study is the use of dilute aluminosilicate solution to control cancrinite growth on sodalite (to suppress the spontaneous nucleation in solution and promote only heteroepitaxial growth on the sodalite surface). The author also showed the heteroepitaxial growth of chabazite on a sodalite substrate whilst maintaining the relation of chabazite (111) // sodalite {111}, as shown in Fig. 5(b).[53)] In this contribution, a unique patterned surface-texture is obtained in the millimeter-scale because of the twin formation of chabazite.

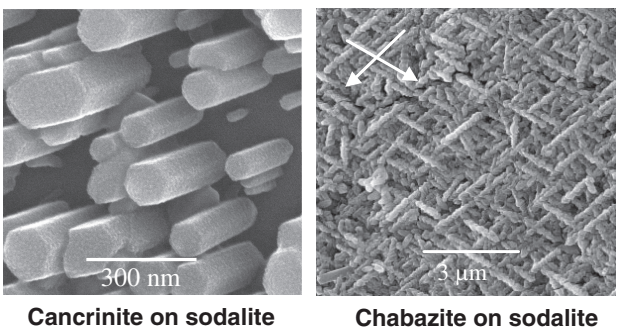

Fig. 5. Heteroepitaxial growth of cancrinite and chabazite on sodalite, respectively.

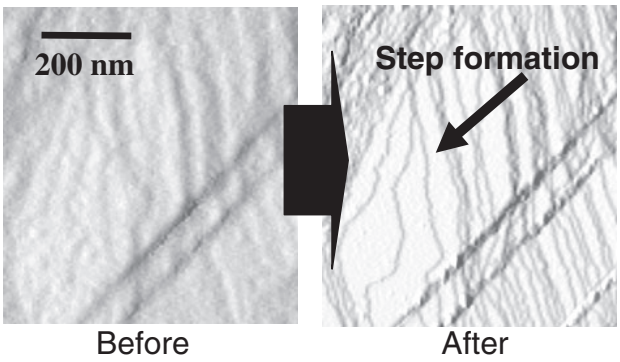

Fig. 6. AFM images at the same position before and after the hydrothermal treatment. Step formation was confirmed after the treatment.

Such a dilute aluminosilicate solution is also useful in preparing clean zeolite surfaces without amorphous matter on an atomic scale. Recrystallization of zeolite [faujasite (Si/Al = 1.2)] surface was performed using dilute aluminosilicate solution with the composition of $405Na_2O{:}1Al_2O_3{:}51SiO_2{:}29900H_2O$. The importance of this particular ratio is that it gives a solution nearly in equilibrium with the faujasite. This means that faujasite is in neither macroscopic growth nor dissolution mode. In these conditions poorly crystalline parts of faujasite are more easily dissolved than the more crystalline parts and tend to recrystallized back onto the faujasite giving a more ordered surface. AFM images at the same position of faujasite before and after the treatment (**Fig. 6**) show that the rough surface of faujasite changes into a well-ordered face in the solution. This surface ordering proceeded by thermodynamic stabilization of the top-surface structure via the mutual transfer of aluminosilicate species between the solution and solid phases.

4. Synthesis of β-SiAlON from a zeolite[55)–59)]

β-SiAlON ceramics are commonly produced by the reaction sintering of mixtures of Si_3N_4, AlN, and Al_2O_3 over 1500°C. The corrosion resistance of β-SiAlON powder is reduced with the formation of its glassy phase in the sintered body. For this reason, preparation of β-SiAlON powder and its sintering using spark plasma sintering (SPS)[60)] has received considerable attention. β-SiAlON powder is mostly synthesized from mixtures of SiO_2 and Al_2O_3 by carbothermal reduction–nitridation (CRN) over 1400°C. So far, the suitability of various raw material minerals, including kaolinite,[61)] halloysite,[62)] montmorillonite[63)] and bentonite,[64)] has been investigated. These minerals are mainly composed of Si and Al, which they contain uniformly on an atomic scale. However, due to the effects of contamination and the difficulty in controlling compositions in the raw materials, for example the Si/Al ratio, products synthesized using these minerals contain AlN, mullite and 15R polytype as impurity phases. The author, therefore, focused on using a zeolite raw material to avoid these problems. Using a zeolite would enable control of the Si/Al ratio by controlling the starting composition. Furthermore, charge compensation cations (e.g. Na^+, Ca^{2+} and H^+) can be introduced easily and uniformly in zeolite structures by ion exchange procedures since the structure contains many anionic Al sites. First, the author showed the successful syntheses of high-purity β-SiAlON[56),57)] from a mixture of zeolite and carbon by the CRN process; however, the resultant products had a large z-value distribution since the composition of the glassy phase became inhomogeneous due to the formation of mullite during firing;[57)] therefore, gas reduction–nitridation (GRN),

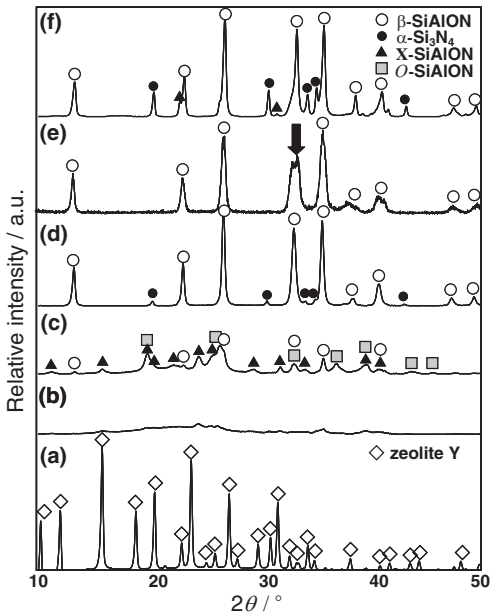

Fig. 7. XRD spectra of (a) raw zeolite, (b) the product synthesized at 1200°C for 0 min, (c) 1400°C for 0 min and (d) 1400°C for 60 min. For comparison, XRD spectra of (e) the product synthesized by the CRN process and (f) the product synthesized from a SiO_2–Al_2O_3 mixture by the GRN process are shown. The arrow indicates that the product has a large distribution of z-values.

which uses a mixture of NH_3 and carbohydrate as a reactant gas (c.a. C_3H_8) was studied for producing high-purity β-SiAlON powder as indicated by the following equations.

$$H_zSi_{6-z}Al_zO_{12}(\text{zeolite}) + (8-z)NH_3 \rightarrow Si_{6-z}Al_zO_zN_{8-z}(\beta\text{-SiAlON}) + (12-z)H_2O \quad (2)$$

The GRN process is quite a simple process since it does not require mixing, milling or a decarburization process. Moreover, the GRN process is generally performed at lower temperatures (1200–1400°C) and with a lower solid solution of carbon in the products than the CRN process (1400–1500°C).

Figure 7 shows XRD spectra of the products synthesized at 1200 and 1400°C for 0 min and 1400°C for 60 min from raw zeolite (HSZ-330HUA, Toso Chem. Co., Tokyo), the product synthesized by the CRN process from the raw zeolite and the product synthesized from the SiO_2–Al_2O_3 mixture by the GRN process. It was found that raw zeolite was transformed into its amorphous phase at 1200°C [Fig. 7(b)] and a small amount of O′-SiAlON and X′-SiAlON as intermediate phases were confirmed in the sample synthesized at 1400°C for 0 min [Fig. 7(c)]. Finally, high-purity β-SiAlON was obtained by heat treatment at 1400°C for 60 min as shown in Fig. 7(d). Figure 7(e) shows the XRD spectrum of the sample prepared by the CRN process. It is found that high purity β-SiAlON can also be synthesized by the CRN process; however, the peak of β-SiAlON is broadened as indicated by the arrow in Fig. 7(e). This indicates that the resultant products have a large distribution of z-values ($0.1 < z < 2.7$) because of the formation of a Si-rich amorphous phase and an Al-rich mullite phase during firing and subsequent crystallization to β-SiAlON.[57)] Note that The z value of the β-SiAlON phase was the mean of z_a and z_c calculated from the cell parameters by the following equations.

$$a = 7.603 + 0.0296z\,\text{Å} \quad c = 2.907 + 0.0255z\,\text{Å} \quad (3)$$

Figure 7(f) shows the XRD spectrum of the product prepared from the SiO_2–Al_2O_3 mixture. It was found that α-Si_3N_4 represents a considerable impurity phase when compared to zeolite as raw material [Fig. 7(d)]. This result can be ascribed to inhomogeneous distributions of Si and Al atoms in the SiO_2–Al_2O_3 mixture. It is known that SiO gas is formed in a reducing atmosphere around 1400°C. Because the Si and Al atoms are not distributed uniformly on an atomic scale in the SiO_2–Al_2O mixture, SiO gas is easily formed and reacts with NH_3. As a result, a larger volume of α-Si_3N_4 is formed as indicated by the following equations.

$$SiO_2 + 2NH_3 \rightarrow SiO + N_2 + H_2O + 2H_2 \quad (4)$$

$$3SiO + 4NH_3 \rightarrow Si_3N_4 + 3H_2O + 3H_2 \quad (5)$$

On the other hand, since Si and Al atoms are mixed uniformly on an atomic scale in zeolite, it is thought that uniform reaction was performed at lower temperature (1200–1400°C) and the formation of SiO gas is prevented by well-dispersed Al atoms in the amorphous phase, suppressing α-Si_3N_4 formation and forming high purity β-SiAlON powder with a sharp z-value distribution ($z = 1.5$).

As a result, high purity β-SiAlON powder was produced from zeolite by GRN at 1400°C for 60 min. Zeolite was used directly as the raw material without previous preparation or handling. Furthermore, completely pure β-SiAlON was produced successfully, containing no minor phases, by the optimization of nitridation, that is, by concentration of C_3H_8 and the timing of its introduction, and its formation mechanism was investigated in detail by ^{27}Al and ^{29}Si NMR.[59)]

5. Conclusions

Zeolites and SiAlONs have been synthesized and characterized. This study draws the following conclusions:

(1) The application of a HEXRD technique for the elucidation of zeolite crystallization has been performed for the first time and clear changes are confirmed in the medium-range order, especially in the formation of aluminosilicate rings in the initial stages of zeolite crystallizations.
(2) Heteroepitaxial growth of cancrinite and chabazite on sodalite has been performed. A characteristic point of the study is the use of dilute aluminosilicate solution to control cancrinite growth on sodalite. Furthermore, it is possible to obtain a well-ordered zeolite surface using the same solution.
(3) High purity β-SiAlON powder was produced from a zeolite by GRN at 1400°C for 60 min. Zeolite was used directly as the raw material without previous preparation or handling.

Acknowledgments The author gratefully acknowledges Professor Tatsuya Okubo of The University of Tokyo for his helpful suggestions and comments, and for his kind support in presenting the work. The author also wishes to express his sincere gratitude to Professors Katsutoshi Komeya, Takeshi Meguro and Junichi Tatami of Yokohama National University for their contribution to fruitful discussions on the present work.

References

1) D. W. Breck, "Zeolite Molecular Sieves", Wiley, New York (1974).
2) R. M. Barrer, "Hydrothermal Chemistry of Zeolites", Academic Press, London (1982).
3) T. Wakihara and T. Okubo, *Chem. Lett.*, **34**, 276–281 (2005).
4) C. S. Cundy and P. A. Cox, *Chem. Rev.*, **103**, 663–701 (2003).
5) http://www.iza-structure.org.
6) S. Kasahara, K. Itabashi and K. Igawa, *Stud. Surf. Sci. Catal.*, **28**, 185 (1986).
7) J. A. Rabo and M. W. Schoonover, *Appl. Catal., A*, **222**, 261–275 (2001).
8) M. E. Davis, *Nature*, **417**, 813–821 (2002).
9) Y. Nozue, T. Kodaira and T. Goto, *Phys. Rev. Lett.*, **68**, 3789–3792 (1992).
10) G. Ihlein, F. Schüth, O. Krauss, U. Vietze and F. Laeri, *Adv. Mater.*, **10**, 1117–1119 (1998).
11) P. Yang, G. Wirnsberger, H. C. Huang, S. R. Cordero, M. D. McGhee, B. Scott, T. Deng, G. M. Whitesides, B. F. Chmelka, S. K. Buratto and G. D. Stucky, *Science*, **287**, 465–467 (2000).
12) Y. Wada, T. Okubo, M. Ryo, T. Nakazawa, Y. Hasegawa and S. Yanagida, *J. Am. Chem. Soc.*, **122**, 8583–8584 (2000).
13) S. Hampshire, H. K. Park, D. P. Thompson and K. H. Jack, *Nature*, **274**, 880 (1978).
14) C. L. Hewett, Y.-B. Cheng, B. C. Muddle and M. B. Trigg, *J. Am. Ceram. Soc.*, **81**, 1781–1788 (1998).
15) C. L. Hewett, Y.-B. Cheng, B. C. Muddle and M. B. Trigg, *J. Eur. Ceram. Soc.*, **18**, 417–427 (1998).
16) T. Wakihara, S. Kohara, G. Sankar, S. Saito, M. Sanchez-Sanchez, A. R. Overweg, W. Fan, M. Ogura and T. Okubo, *Phys. Chem. Chem. Phys.*, **8**, 224–227 (2006).
17) T. Wakihara, Y. Suzuki, W. Fan, S. Saito, S. Kohara, G. Sankar, M. Sanchez-Sanchez, M. Ogura and T. Okubo, *J. Ceram. Soc. Japan*, **117**, 277–282 (2009).
18) T. Wakihara, W. Fan, Y. Suzuki, M. Ogura, S. Kohara, G. Sankar and T. Okubo, *Stud. Surf. Sci. Catal.*, **170**, 506–511 (2007).
19) T. Wakihara, W. Fan, S. Kohara, M. Ogura, G. Sankar and T. Okubo, *Chem. Lett.*, **37**, 30–31 (2008).
20) T. Wakihara, K. Sato, S. Kohara, G. Sankar, J. Tatami, K. Komeya, T. Meguro and K. J. D. MacKenzie, *Microporous Mesoporous Mater.*, **136**, 92–96 (2010).
21) C. S. Cundy and P. A. Cox, *Microporous Mesoporous Mater.*, **82**, 1–78 (2005).
22) M. T. Melchior, D. E. W. Vaughan and C. F. Pictroski, *J. Phys. Chem.*, **99**, 6128–6144 (1995).
23) A. T. Bell, *Colloids Surf., A*, **158**, 221–234 (1999).
24) M. Ogura, Y. Kawazu, H. Takahashi and T. Okubo, *Chem. Mater.*, **15**, 2661–2667 (2003).
25) J. S. Beck, J. C. Vartuli, G. J. Kennedy, C. T. Kresge, W. J. Roth and S. E. Schramm, *Chem. Mater.*, **6**, 1816–1821 (1994).
26) S. L. Burkett and M. E. Davis, *J. Phys. Chem.*, **98**, 4647–4653 (1994).
27) A. T. Davies, G. Sankar, C. R. A. Catlow and S. M. Clark, *J. Phys. Chem.*, **101**, 10115–10120 (1997).
28) A. Gualtieri, P. Norby, G. Artioli and J. Hanson, *Phys. Chem. Miner.*, **24**, 191–199 (1997).
29) A. Gualtieri, P. Norby, G. Artioli and J. Hanson, *Microporous Mater.*, **9**, 189–201 (1997).
30) A. Iwasaki, T. Sano and Y. Kiyozumi, *Microporous Mesoporous Mater.*, **25**, 119–126 (1998).
31) S. Mintova and V. Valtchev, *Microporous Mesoporous Mater.*, **5**, 171–179 (2002).
32) B. J. Scheman, J. Sterte and J. E. Otterstedt, *Zeolites*, **14**, 110–116 (1994).
33) K. A. Carrado, P. Thiyagarajan and K. Song, *Clay Miner.*, **32**, 29–40 (1997).
34) P. P. E. A. de Moor, T. P. M. Beelen, B. U. Komanschek, L. W. Beck, P. Wagner, M. E. Davis and R. A. van Santen, *Chemistry*, **5**, 2083–2088 (1999).
35) P. P. E. A. deMoor, T. P. M. Beelen and R. A. van Santen, *Microporous Mater.*, **9**, 117–130 (1997).
36) J. N. Watson, L. E. Iton, R. I. Keir, J. C. Thomas, T. L. Dowling and J. W. White, *J. Phys. Chem. B*, **103**, 10094–10104 (1997).

37) P. P. E. A. de Moor, T. P. M. Beelen and R. A. van Santen, *J. Phys. Chem. B*, 103, 1639–1650 (1999).
38) Z. Liu, T. Ohsuna, O. Terasaki, M. A. Camblor, M. J. Diaz-Cabañas and K. Hiraga, *J. Am. Chem. Soc.*, 123, 5370–5371 (2001).
39) V. Alfredsson, T. Ohsuna, O. Terasaki and J. O. Bovin, *Angew. Chem., Int. Ed. Engl.*, 32, 1210–1213 (1993).
40) C. Li, G. Xiong, J. K. Liu, P. L. Ying, Q. Xin and Z. C. Feng, *J. Phys. Chem. B*, 105, 2993–2997 (2001).
41) P. K. Dutta, D. C. Shieh and M. Puri, *J. Phys. Chem.*, 91, 2332–2336 (1987).
42) G. Xiong, Y. Yu, Z. Feng, Q. Xin, F. Xiao and C. Li, *Microporous Mesoporous Mater.*, 42, 317–323 (2001).
43) P. K. Dutta and D. C. Shieh, *J. Phys. Chem.*, 90, 2331–2334 (1986).
44) A. L. Weisenhorn, J. E. Mac Dougall, S. A. C. Gould, S. D. Cox, W. S. Wise, J. Massie, P. Maivald, V. B. Elings, G. D. Stucky and P. K. Hansma, *Science*, 247, 1330–1333 (1990).
45) M. W. Anderson, J. R. Agger, J. T. Thornton and N. Forsyth, *Angew. Chem., Int. Ed. Engl.*, 35, 1210–1213 (1996).
46) J. R. Agger, N. Pervaiz, A. K. Cheetham and M. W. Anderson, *J. Am. Chem. Soc.*, 120, 10754–10759 (1998).
47) S. Sugiyama, S. Yamamoto, O. Matsuoka, H. Nozoye, J. Yu, G. Zhu, S. Qiu and O. Terasaki, *Microporous Mesoporous Mater.*, 28, 1–7 (1999).
48) S. Kohara, K. Suzuya, K. Takeuchi, C. K. Loong, M. Grimsditch, J. K. R. Weber, J. A. Tangeman and T. S. Key, *Science*, 303, 1649–1652 (2004).
49) G. Sankar, J. M. Thomas and C. R. A. Catlow, *Top. Catal.*, 10, 255–264 (2000).
50) G. Xiong, Y. Yu, Z. C. Feng, Q. Xin, F. S. Xiao and C. Li, *Microporous Mesoporous Mater.*, 42, 317–323 (2001).
51) T. Shiraki, T. Wakihara, M. Sadakata, M. Yoshimura and T. Okubo, *Microporous Mesoporous Mater.*, 42, 229–234 (2001).
52) T. Okubo, T. Wakihara, J. Plévert, S. Nair, M. Tsapatsis, Y. Ogawa, H. Komiyama, M. Yoshimura and M. E. Davis, *Angew. Chem., Int. Ed.*, 40, 1069–1071 (2001).
53) T. Wakihara, S. Yamakita, K. Iezumi and T. Okubo, *J. Am. Chem. Soc.*, 125, 12388–12389 (2003).
54) T. Wakihara, A. Sugiyama and T. Okubo, *Microporous Mesoporous Mater.*, 70, 7–13 (2004).
55) T. Wakihara, S. Kamiwaki, J. Tatami, K. Komeya and T. Meguro, *J. Ceram. Soc. Japan*, 115, 294–296 (2007).
56) F. J. Li, T. Wakihara, J. Tatami, K. Komeya and T. Meguro, *J. Eur. Ceram. Soc.*, 27, 2535–2540 (2007).
57) F. J. Li, T. Wakihara, J. Tatami, K. Komeya, T. Meguro and K. J. D. Mackenzie, *J. Am. Ceram. Soc.*, 90, 1541–1544 (2007).
58) T. Yamakawa, T. Wakihara, J. Tatami, K. Komeya and T. Meguro, *J. Ceram. Soc. Japan*, 116, 325–328 (2008).
59) T. Wakihara, Y. Saito, J. Tatami, K. Komeya, T. Meguro, K. J. D. Mackenzie, S. Takagi and M. Yokouchi, *J. Ceram. Soc. Japan*, 116, 980–983 (2008).
60) Q. Li, K. Komeya, J. Tatami, T. Meguro and L. Gao, *Key Eng. Mater.*, 247, 75 (2006).
61) H. L. Lee, H. J. Lim, S. Kim and H. B. Lee, *J. Am. Ceram. Soc.*, 72, 1458–1461 (1989).
62) K. J. D. Mackenzie, R. H. Meinhold, G. V. White and C. M. Sheppard, *J. Mater. Sci.*, 29, 2611–2619 (1994).
63) Y. Sugahara, K. Kuroda and C. Kato, *J. Am. Ceram. Soc.*, 72, C-247 (1984).
64) A. D. Mazzoni and E. F. Aglietti, *Appl. Clay Sci.*, 17, 127–140 (2000).

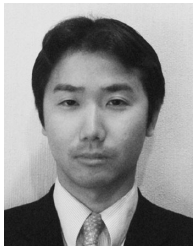

Dr. Toru Wakihara received his Engineering degree from The University of Tokyo, School of Engineering in 1999. He completed his Graduate thesis in 2001 in the Department of Chemical System Engineering, Graduate School of Engineering, The University of Tokyo. He completed his doctoral thesis in the same department in 2004. In 2004, Dr. Wakihara took up a post as Research Associate in the Graduate School of Environment and Information Sciences at Yokohama National University where his main topics of research were nitride, oxynitride, carbide and ceramic processing and also zeolites. In 2007, he was appointed Assistant Professor at Yokohama National University.